PAPER

Check for updates

Laser-based ion doping is a suitable alternative to dope biologically active ions into colloidal bioglass nanoparticles†

Pichaporn Sutthavas, [ID] [a] Matthias Schumacher,[a] Martyna Nikody, [ID] [ab] Vaijayanthi Ramesh,[c] Jurij Jakobi,[c] Elizabeth R. Balmayor, [ID] [ad] Pamela Habibovic, [ID] [a] Christoph Rehbock,[c] Stephan Barcikowski [ID] *[c] and Sabine van Rijt [ID] *[a]

Bioactive glass nanoparticles (nBGs) have demonstrated promising properties for bone regeneration due to their bone-binding ability. Incorporating multiple ions into nBGs can improve their bioactivity and provide them with additional functionalities aiding bone repair. However, incorporating multiple ions into nBGs combining different functionalities is still challenging as the additional ions often interfere with the nanoparticle properties. To overcome these challenges, here we report the use of pulsed laser doping and co-doping techniques as an alternative method for ion incorporation into colloidal nBGs. We demonstrate the simultaneous laser-induced incorporation of iron (Fe), strontium (Sr), and/or copper (Cu) ions into nBGs from simple salt solutions without altering the particles' morphology. Furthermore, laser-doped nBGs were biocompatible and could significantly increase alkaline phosphatase (ALP) production in human mesenchymal stromal cells (hMSC). Moreover, laser-*co*-doped nBGs containing Fe and Sr ions significantly increased vessel formation by human umbilical vein endothelial cells (HUVEC). Therefore, pulsed laser doping in liquids was shown to be a versatile technique to incorporate multiple ions into nBGs and allow systematic studies on cooperative effects of dopants in active biomaterials.

Introduction

Bioactive glass nanoparticles (nBGs) are extensively researched in the bone regenerative medicine field due to their inherent bioactivity and bone-bonding capabilities.[1] nBGs consist of a silica network containing calcium and phosphate ions, creating an open glass structure. The extent of calcium and phosphate present in the glass plays an important role in their biodegradation rate and bioactivity. Specifically, the dissolution of the particles and subsequent silica, calcium, and phosphate ion

release can promote osteogenic processes (stem cell differentiation towards mature osteoblasts). Moreover, silica ions are known to promote angiogenesis (*de novo* formation of blood vessels).[2] Due to their small size, ranging from 20 to 800 nm, nBGs have been used as components in scaffolds, coatings, and drug delivery vehicles.[3]

The incorporation of additional ions into nBGs (*i.e.* ion doping) such as copper (Cu), strontium (Sr), and zinc (Zn) can be used to further improve their bioactivity or add new functionalities.[2,4] For example, the incorporation of metallic dopants such as silver and gold could infer antibacterial properties to the nBGs particles.[5,6] Furthermore, Cu doping improved nBGs angiogenic properties, whereas Sr and Zn doping has been used to improve nBGs osteogenic activity.[7–9] Wet synthesis methods are generally used to dope nBGs with ions by mixing ionic salts with silica precursors. However, the selection of ions, doping ratio, and synthesis protocol highly influence nBGs formation, and can (negatively) influence their morphology, homogeneity, and biodegradation rate.[10] Moreover, ion doping *via* sol–gel wet synthesis is limited in the number and amounts of ions that can be doped before nBGs are negatively influenced, and discrepancies between the intended and actual doping amounts frequently occur.[11] Finally, with current

[a] Department of Instructive Biomaterials Engineering, MERLN Institute for Technology-Inspired Regenerative Medicine, Maastricht University, P.O. Box 616, 6200 MD Maastricht, The Netherlands. E-mail: s.vanrijt@maastrichtuniversity.nl

[b] Department of Complex Tissue Regeneration, MERLN Institute for Technology-Inspired Regenerative Medicine, Maastricht University, P.O. Box 616, 6200 MD Maastricht, The Netherlands

[c] Technical Chemistry I and Center for Nanointegration Duisburg-Essen (CENIDE), University of Duisburg Essen, Universitaetsstr.2, 45141 Essen, Germany. E-mail: stephan.barcikowski@uni-due.de

[d] Experimental Orthopaedics and Trauma Surgery, Department of Orthopaedic, Trauma, and Reconstructive Surgery, RWTH Aachen University Hospital, Aachen, Germany

† Electronic supplementary information (ESI) available. See DOI: https://doi.org/10.1039/d3ma00112a

methods, it is difficult to dope multiple ions simultaneously in single nBGs particles and ion distribution inside the nBGs matrix may be impaired.

Reactive laser processing of colloids has emerged as an alternative method in the last few years and was recently reviewed by the Tibbets group.[12] Process variants are irradiation of precursor solutions in liquids (reductive laser synthesis in liquids), ablation of a bulk target in the presence of an ionic precursor solution (reactive laser ablation in liquids), or irradiation of a nanoparticle or microparticle suspension in the presence of ionic precursors.[12] One sub-field of reactive laser synthesis in liquids is laser doping, where not nanoparticles but single atoms from a liquid are incorporated into the base material, a process usually favored by low precursor concentrations. For example, the laser ablation of a Gd_2O_3 target in a Eu^{3+} solution yielded doped materials with a characteristic visible fluorescence.[13] Other studies describe the incorporation of single atoms of gold and nickel into metallic $Ru^{14,15}$ or silver into Ir.[16] Recently Zerebecki *et al.* reported laser-induced doping of Fe ions into Co_3O_4 by applying low fluence laser heating and precisely controlling the number of laser pulsed per colloid volume.[17] Laser-based doping of bioactive glass (BG) on the other hand has been rarely explored. In one study Li and Ramesh *et al.* examined the reactive laser fragmentation of micrometer-sized 45S5 BG in the presence of Cu (EDTA) and Fe (EDTA) complex solutions. Fe and Cu could be incorporated into the BG network, however, simultaneous reduction of particle size was observed.[18]

Major advantages of the pulsed laser doping method include the facile control of doping levels by ion concentrations as well as the possibility for homogeneous ion incorporation. In previous work, laser doping of BG was only observed together with a laser fragmentation induced size reduction effect.[18] This size reduction increased the total surface area of the BG colloids as the mass remained constant. This, however, makes it impossible to differentiate a doping effect by the laser and stronger adsorption of the metal ions due to a larger available surface area. Thereto, in this work we chose a two-step approach, generating nBGs by established sol–gel chemistry and consecutively irradiating the nBGs suspension by a nanosecond-pulsed, kilohertz-repetition-rate UV laser in salt solutions, choosing irradiation conditions that do not affect particle size and guarantee that the particle surface area remains constant. Furthermore, we extended the range of ions utilizing Sr^{2+} due to its known osteogenic activity and Cu^+ and Fe^{2+} as they support angiogenesis.[19–22] The ability of doped nBGs to stimulate angiogenesis was investigated using a tubular formation assay. Moreover, we investigated whether ion doped nBGs showed improved osteogenic bioactivity by assessing ALP levels and ability to promote matrix production in hMSCs.

Results and discussion

nBGs synthesis and metal ion doping

nBGs particles with glass composition of $SiO_2/CaO/P_2O_5 = 80/15/5$ mol-% were synthesized using a base-catalyzed sol–gel process, and subsequently calcined at 600 °C, similar to what we reported previously.[23] Uniform round-shaped nanosized nBGs particles were obtained as shown by TEM (Fig. 1a). Fourier transform-infrared (FTIR) spectrum of the nBGs particles displayed a peak at ~ 400 and ~ 1000 cm^{-1} characteristic for the Si–O bond (Fig. 1b). Moreover, XRD analysis showed that nBGs particles were amorphous (Fig. 1c). Laser doping was conducted using the nanosecond UV laser irradiating the free liquid jet of the passage reactor (30 passages for each sample). The 20 wt% nBGs suspensions were exposed to initial Fe : Cu : Sr molar ratios of (A) 1 : 1.5 : 1.5, (B) 1 : 3 : 0, (C) 1 : 0 : 3. Furthermore, a control immersed in a 1 : 1.5 : 1.5 solution was processed. Fe-EDTA solutions with a pronounced UV extinction at 355 nm (laser wavelength) were used to ensure an efficient absorbance of the laser energy by the sample. Fig. 2 shows exemplary SEM images of the raw and doped samples. Number-weighted particle size distributions obtained from these images indicate a mean value of 124.7 ± 11.3 nm before and 127.5 ± 13.6 nm after laser processing, which indicates that particle size was not significantly affected by the laser processing.

Next, we analyzed the elemental composition of the doped nBGs. The Si content as the major network-forming element was unaffected by the doping (Fig. 3a), which is to be expected as minor changes in the composition of the dominant element may not have been detectable with sufficient accuracy. For the major network modifier Ca, a reduction of about 50% for all doped and immersed samples was found. This may be due to the presence of EDTA in the samples, which could have initiated Ca leaching by complexation, as documented *e.g.* for hard tissue decalcification.[24] Moreover, we observed that Fe, Cu, and Sr were present in the doped nBGs particles showing that the laser treatment was effective. In contrast, no ion concentrations could be detected in immersed nBGs, likely because of unsuccessful or too low ion incorporation in the absence of a laser beam. Examination of the doping levels of the corresponding elements revealed that in Fe:Cu doped nBGs, higher levels of Cu were embedded compared to Fe, which was to be expected as the Fe : Cu ratio in the experiment was 1 : 3. Recently, laser fragmentation mechanisms have been studied for single microparticles, pointing at a photomechanical contribution to the fragmentation[25] not to be expected for smaller particles (such as nBGs) as those are unlikely to fulfill the stress confinement criteria for nanosecond pulses. Hence, nanosecond-pulsed
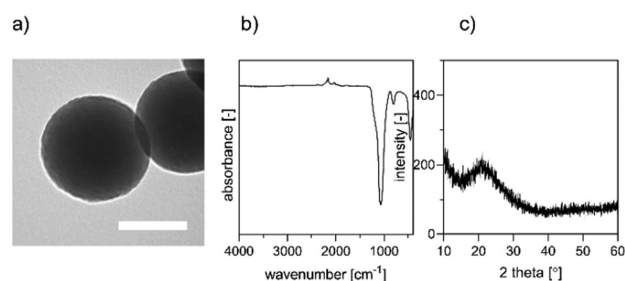

Fig. 1 Characterization of nBGs; (a) morphology of synthesized nBGs by TEM. Scale bar represents 100 nm (b) FTIR spectra of the nBGs (c) X-ray diffraction patterns of nBGs.
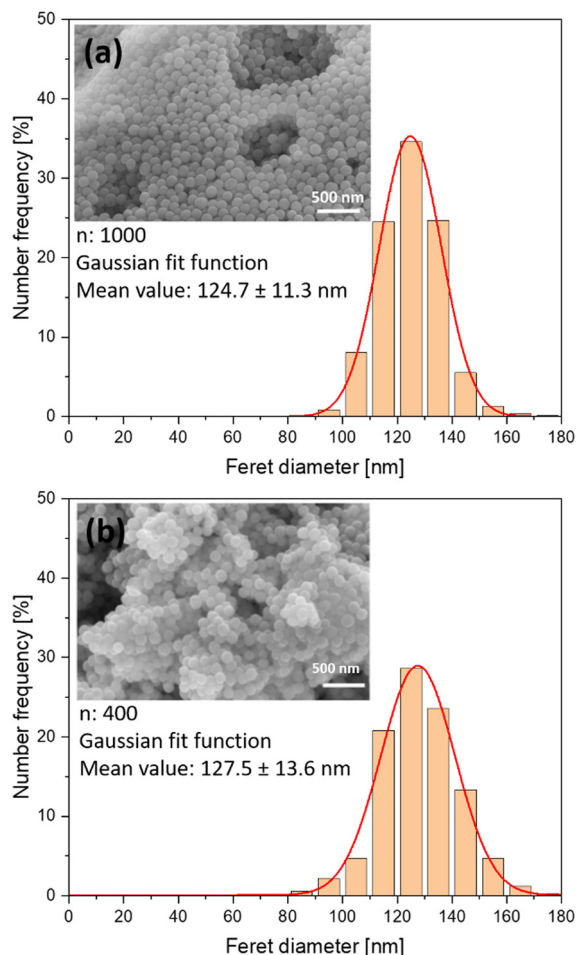
Fig. 2 Number-weighted particle size distributions and exemplary SEM images of (a) raw nBGs and (b) nBGs laser-doped with Fe:Cu:Sr. Distributions.

laser excitation of nBGs dispersed in metal salts or metal salt mixtures results in homogeneous doping or co-doping of the metals into the nBGs volume, without changing the host particle size, albeit with relatively low ion doping levels.

This is in contrast to our previous work using micrometer-sized BG particles,[18] where size reduction was observed. Thus, the laser-based ion doping technique allows us to evaluate doping effects independently from particle size effects. Conventional co-precipitation methods for nBGs ion doping can also afford effective ion loading of Cu, Fe and Sr.[28,29] However, depending on ion concentration and synthesis conditions, this method can negatively impact nBGs formation, structure, and morphology.[11] Especially incorporation of Fe in BG has resulted in the formation of particle agglomerates and can negatively influence nanoparticle structure.[30,31] Thus, the laser-doping technique demonstrated here can present advantages over current precipitation techniques.

Biocompatibility and induction of ALP levels

The biocompatibility of immersed nBGs, FeCu, and FeCuSr laser-doped nBGs was assessed in hMSCs after 72 hours of exposure to concentrations ranging from 25 to 100 μg mL^{-1} using the MTT assay (Fig. 4a). None of the conditions tested resulted in a significant change in hMSCs metabolic activity compared to control cells. These results indicate that both, immersed and laser-doped nBGs were biocompatible with hMSCs at the concentrations tested. This was confirmed by performing live/dead staining and fluorescent microscopy (Fig. S4, ESI†); hMSCs exposed to 50 or 100 μg mL^{-1} of FeCu, FeCuSr and Immersed nBGs for 72 hours were confluent with elongated morphology and with minimal signal for ethidium bromide (stains apoptotic cells). Next, the ability of the nBGs and laser-doped nBGs nanoparticles to induce ALP activity, a known marker for hMSC osteogenic differentiation, was assessed. After 7 days of incubation, no significant ALP activity was measured in any of the sample conditions. Significant ALP production was observed after 14 and 21 days of exposure for all samples tested although lower compared to the positive control (OM). The ALP activity in hMSCs exposed to nBGs, immersed nBGs, and FeCuSr laser doped nBGs after 14 days was similar; 2.14 fold (in comparison to control) for nBGs, 2.02 fold for immersed nBGs, and 2.12 fold for FeCuSr laser doped nBGs. hMSC exposed to FeCu and FeSr laser-doped nBGs also led to increased ALP production albeit significantly lower compared to the other sample conditions (1.49 fold for FeCu and 1.48 fold for FeSr). After 21 days, overall ALP levels were higher than after 14 days and showed a similar trend; exposure to immersed nBGs, and FeCuSr laser-doped nBGs resulted in similar ALP production (4.16 fold for nBGs, 4.1 fold for immersed nBGs, and 3.94 fold for FeCuSr nBGs) and significant albeit lower ALP production for FeCu and FeSr laser doped nBGs was observed (2.69 fold for FeCu and 3.22 fold for FeSr laser doped nBGs). Next, we investigated whether nBGs, immersed and laser-doped nBGs nanoparticle exposure could promote the ability of hMSCs to mineralize their extracellular matrix, an important step in *de novo* bone formation. Calcium deposition by differentiated

UV laser excitation of nanoparticles in the low fluence regime applied here is most likely linked to a particle-surface-heating process, causing pulsed-laser-induced diffusion enhancement.[17] Furthermore, ion uptake specificity (higher affinity of Fe than Cu as found in[18]) seems to be less pronounced (not dominant) at lower doping levels or in case no size reduction occurs. Upon co-doping with Sr, the Fe doping levels drastically increased by a factor of 9, so the presence of Sr seemed to promote Fe doping. This may be attributed to the overall larger ionic radius of Sr^{2+} in comparison to Ca^{2+},[26,27] widening the BG network and promoting the uptake of other ions such as Fe. In the case of the Cu:Fe:Sr co-doping we found a higher doping level of Fe in comparison to Cu, which is in accordance with our previous findings.[18] Finally, we probed for the presence of Fe, Cu, and Sr in nBGs on a single particle level using TEM-EDX (Fig. 3(c) and (d)) and found a moderate accumulation of the corresponding ions in the particles, although total doping levels were low. The distribution of the elements as determined by TEM-EDX mapping of the particles in Fig. 3 was homogeneous. Fe, Sr or Cu doping did not lead to alterations in nanoparticle morphology as observed by TEM, SEM and FTIR (Fig. S1–S3, ESI†). Overall, the nanosecond UV
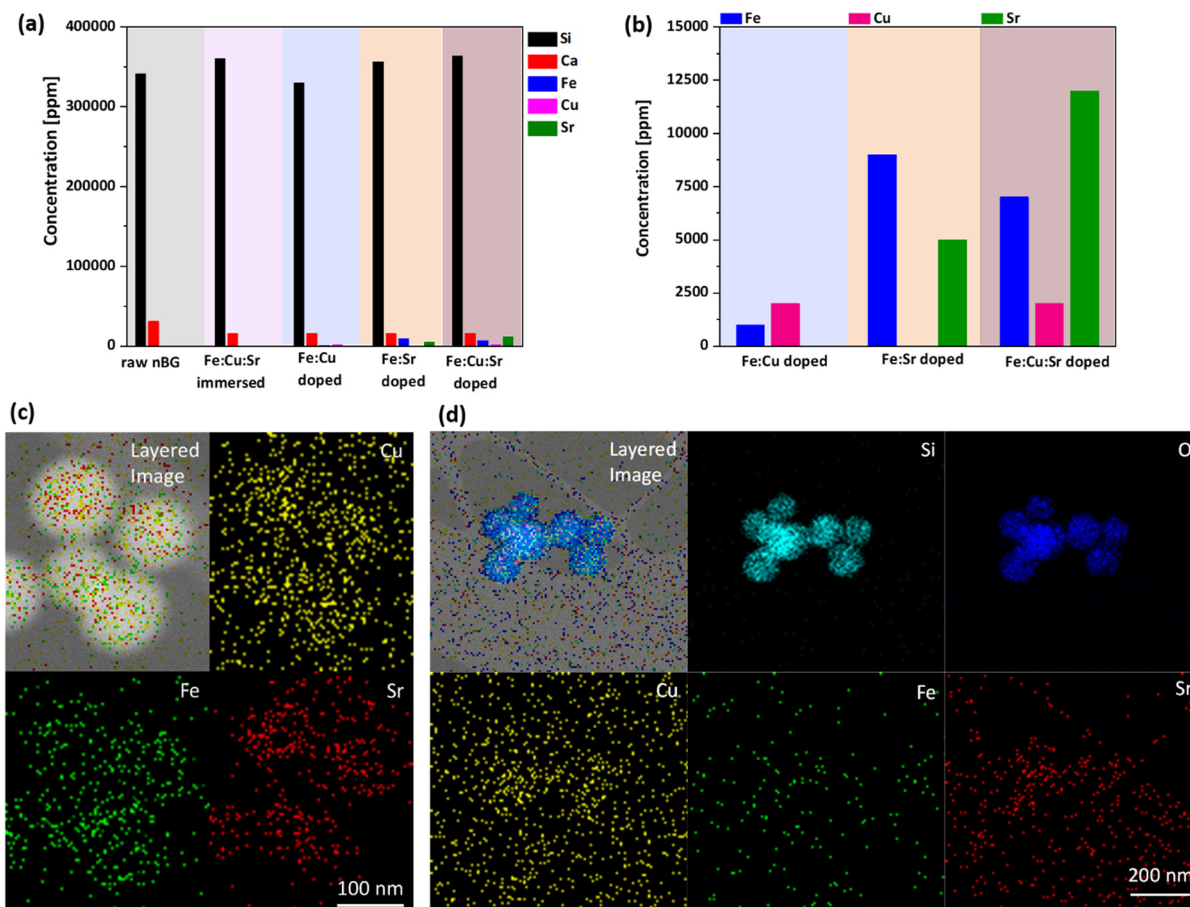
Fig. 3 Particle composition: SEM-EDX ensemble measurements of (a) all elements and (b) Fe, Cu, and Sr present in laser-doped samples. TEM-EDX elemental mapping of (c) Fe, Cu, Sr doped and (d) Fe, Cu, Sr immersed samples.

hMSCs was determined after 28 days using Alizarin Red S Staining (Fig. 5). hMSC cultured in basic and mineralization media (MM) in the absence of nanoparticles were used as negative and positive controls, respectively. nBGs, immersed and laser-doped nBGs exposure to hMSCs led to significant calcium deposition, however, significantly less compared to the positive control (Fig. 5). Further quantification of the staining revealed that similar mineralization production was observed for hMSCs exposed to nBGs, immersed nBGs, FeSr, and FeCuSr laser-doped nBGs (Fig. 5b). In contrast, hMSCs exposed to FeCu laser-doped nBGs resulted in the lowest calcium deposition (0.48 mM). In conclusion, laser metal doped nBGs were biocompatible, and did not significantly enhance the osteogenic activity of nBGs particles nor their ability to promote hMSC mineralization. Specifically, non-doped nBGs, immersed nBGs, and nBGs laser-doped with FeCuSr resulted in the induction of similar hMSCs ALP activity levels, and lower ALP levels were observed for FeSr and FeCu-doped nBGs. Similar observations were made for their ability to promote mineralization. The lower ALP and mineralization levels observed after exposure to FeSr and FeCu doped nBGs are likely related to the known effect of Fe on reducing ALP activity in bone cells.[32–34] For example, osteoblasts exposed to 50–200 μM ferric ammonium citrate led to a concentration-dependent decrease of ALP activity and negatively impacted mineralization.[32] Another study showed that high intracellular Fe levels in primary rat bone marrow stem cells led to downregulation of several osteogenic markers such as Runx2, osterix, osteopontin, and osteocalcin, but enhanced proliferation of pre-osteoblasts.[33] Although Sr is known to induce osteogenesis and ALP production in the absence of other osteogenic supplements,[8,35,36] the Fe may negatively influence ALP production, lowering the overall bioactivity of FeSr-doped nBGs. Although Cu is also known to reduce ALP activity of hMSCs and suppress mineralization,[37] FeCuSr doped nBGs showed similar ALP levels compared to undoped nBGs. The differential osteogenic activity of FeSr doped nBGs particles compared to FeCuSr nBGs is likely related to the relatively higher Sr concentration in the latter nanoparticles; Sr doping in the FeCuSr nBGs was more than double compared to FeSr nBGs.

In vitro angiogenesis

To investigate the influence of laser doping of nBGs on their angiogenic properties, HUVECs were cultured with the nBGs incorporated into Geltrex for 12 hours (Fig. 6). Tube-like structure formation was observed in all tested conditions. In comparison with the Geltrex control, the addition of VEGF as well as all tested nBGs resulted in more pronounced tubule formation. Furthermore, cells cultured in the presence of FeSr laser-doped nBGs formed
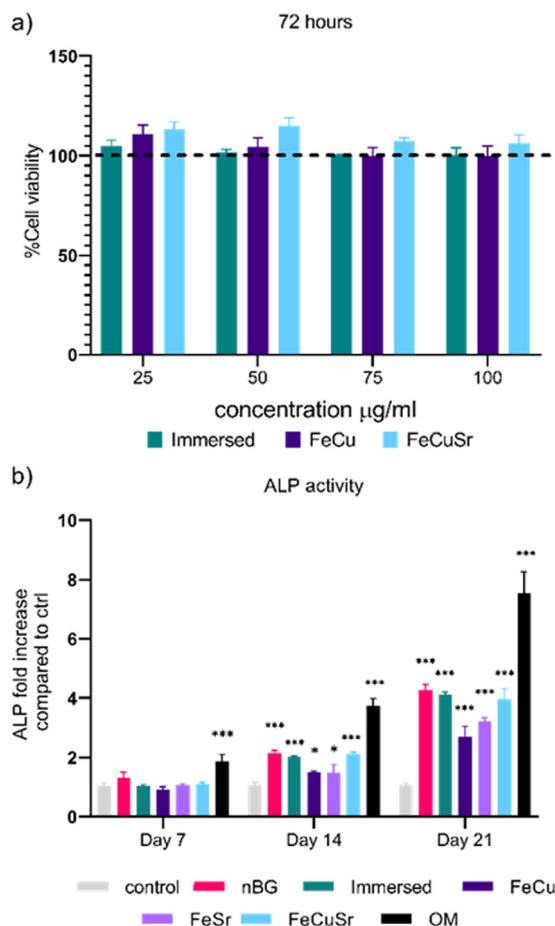
Fig. 4 (a) Metabolic activity of hMSC measured using the MTT assay after 72 hours exposure to 25, 50, 75, and 100 µg mL^{-1} immersed nBGs, FeCu, and FeCuSr laser doped nBGs (depicted as immersed, FeCu and FeCuSr, respectively). The metabolic activity is shown as % compared to control cells. (b) hMSC ALP activity after exposure to 100 µg mL^{-1} of nBGs, immersed nBGs, and FeCu, FeSr, FeCuSr laser doped nBGs. ALP activity was normalized to DNA content. Negative control group are cells cultured in basic media and the positive control are cells cultured in OM media. All conditions were performed in triplicate. Significant differences between samples and negative controls were indicated by *, as * representing p-values as follows; *$p < 0.033$; **$p < 0.02$; ***$p < 0.001$.

smaller loops compared to the other conditions. Quantitative analysis of the network parameters showed a significant increase in the number of junctions and vessel area in the positive control (VEGF exposure) and for HUVECs exposed to FeSr doped nBGs (Fig. 6(b)). Differential activity was observed in the *in vitro* angiogenesis experiments; nBGs doped with FeSr led to significantly increased vessel area and number of junctions compared to the control. Indeed, Fe is known to be able to stimulate angiogenesis and tube formation. For example, one study showed that Fe released from calcium phosphate scaffold enhanced the proliferation of HUVECs, and upregulated VEGF and endothelial nitric oxide synthase (eNOS).[38] Fe-doped octacalcium phosphate nanoparticles also have been shown to promote HUVEC proliferation and upregulate the expression of several angiogenic genes.[22] Moreover, in addition to Sr's well-known ability to induce osteogenesis, Sr can also have a beneficial effect on angiogenesis. In one study,
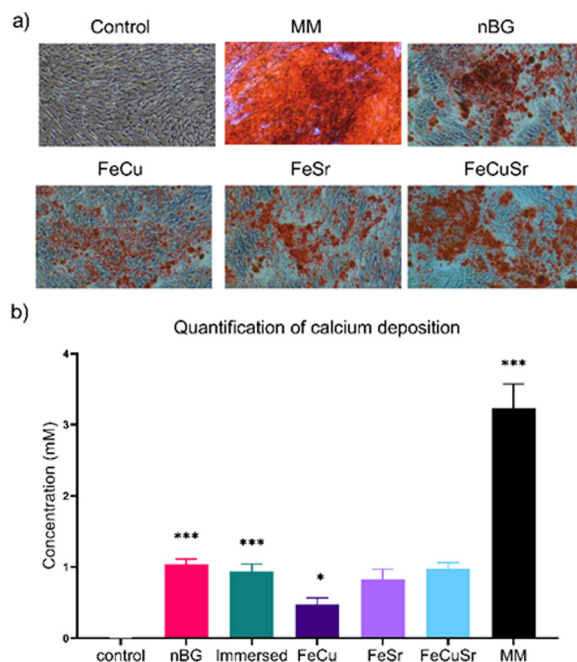

Fig. 5 (a) Calcium deposition by hMSCs at day 28 determined by Alizarin Red staining ($n = 3$); exposed to basic medium, MM medium, non ion-doped nBGs, and laser-doped FeCu, FeSr, and FeCuSr nBGs. (b) Quantification of calcium deposition *via* dye extraction of Alizarin Red. Significant differences between samples and negative controls were indicated by *, as * representing p-values as follows; *$p < 0.033$; **$p < 0.02$; ***$p < 0.001$.

Sr-doped BG sub-microparticles upregulated mRNA expression of angiogenesis-related genes (Angiogenin, FGF-2, and SDF) in HUVECs and increased vascularization within a gelatin scaffold *in vivo*.[39] Although Cu is known to promote angiogenesis, we observed no significant effect of Cu-doped nBGs on *in vitro* sprouting of HUVECs. This is likely due to the low Cu content in our laser-doped nBGs.

Experimental

Synthesis of nano-sized bioactive glass (nBGs) particles

nBGs particles were synthesized by a base-catalyzed sol–gel process.[23] Unless stated otherwise, all synthesis steps were performed at room temperature (RT) while vigorously stirring. First 2.77 g tetraethyl orthosilicate (TEOS) and 0.25 mL triethyl phosphate (TEP) were dissolved in 2.8 mL methanol. After 30 minutes, a mixture of 12.6 mL ddH$_2$O, 29 mL ethanol, and 2.56 mL 25% ammonia was added. After another 60 minutes, 1.57 g CNT were added. After 12 hours, nBGs particles were collected by centrifugation at $1500 \times g$ for 5 minutes and washed in a mixture of methanol and ethanol. The collected particles were vacuum-dried, calcinated at 600 °C for 3 hours with a heating rate of 2 K minute^{-1}, and re-suspended in ethanol at a concentration of 10 mg mL^{-1} for subsequent processing.

Laser *in situ* doping of nBGs particles

Laser-doping was carried out in a liquid-jet flow through a reactor introduced by Lau *et al.*[40] following a procedure
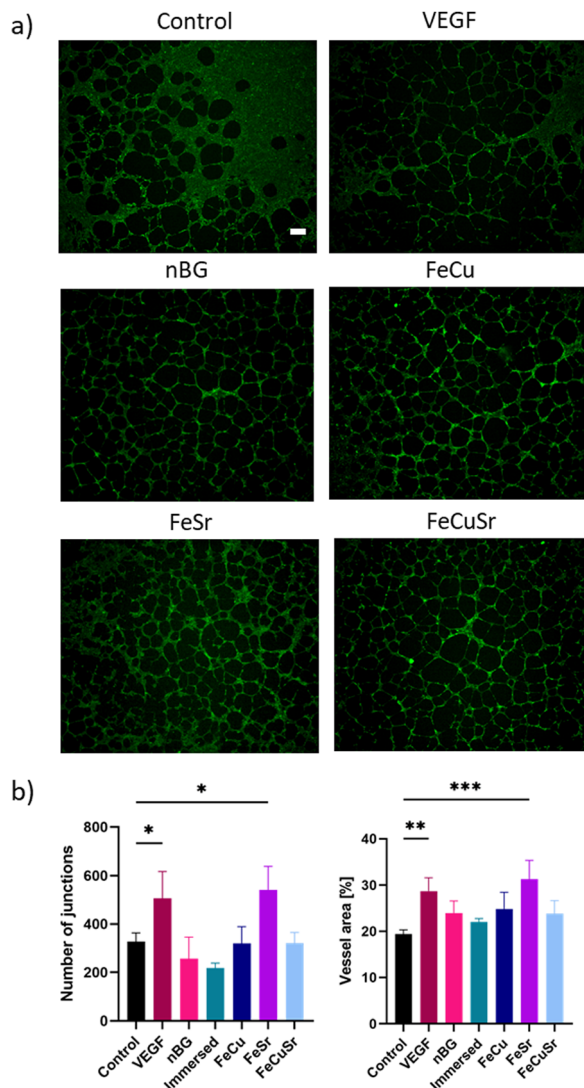
a)

Fig. 6 *In vitro* angiogenesis assay. (a) HUVECs cultured on Geltrex in control and experimental conditions stained with phalloidin (green). Scale bar = 0.25 mm. (b) Quantitative analysis of the number of junctions and vessel area.

described in detail in our previous work.[18] In short, a 20 wt% suspension of nBGs was initially washed three times with deionized water and then dispersed in mixed Fe-EDTA, Cu-EDTA, and $Sr(NO_3)_2$ solutions (178 mM stock solutions) and laser irradiated for 30 passages with a mean volume flow-rate of 0.54 mL s^{-1} using a nanosecond-pulsed laser (Avia 355-14, Coherent, Inc., USA) at a wavelength of λ = 355 nm, a repetition rate of 40 kHz and a laser fluency of 60 mJ cm^{-2}. The irradiated samples had initial Fe : Cu : Sr molar ratios of (A) 1 : 1.5 : 1.5, (B) 1 : 3 : 0, (C) 1 : 0 : 3. Furthermore, a control immersed in a 1 : 1.5 : 1.5 solution was processed similarly in the passage reactor, just without laser irradiation. The processed samples were washed twice in deionized water, twice in ethanol, and finally dispersed in fresh ethanol.

Nanoparticle characterization

Crystallinity of synthesized nBGs were determined by X-ray diffractograms (XRD) using a Bruker D2 Phaser diffractometer (USA) with Cu Kα radiation (λ = 1.5406 Å) in the range of $6 \leq 2\Theta \leq 60°$ in 0.02° increments and with an integration time of 0.75 s. ATR-FTIR (Nicolet iS50, Thermo Scientific, USA) was used to assess functional groups, running 32 scans between 400 and 4000 per cm with a resolution of 0.5 per cm. Spectra were analyzed with Spectragryph (F. Menges, Version12,2018, https://www.effemm2.de/spectragryph.) nBGs' morphology were visualized and assessed using transmission electron microscopy (TEM, FEI Tecnai G2 Spirit BioTWIN iCorr (G0.201), USA). The particle size was determined from TEM images using ImageJ analysis (ImageJ 1.52n). The surface charge of synthesized and modified particles suspended in PBS (0.5 mg mL^{-1}) was evaluated with zeta potential analysis (Malvern Zetasizer Nano, Panalytical, UK). Further characterization of the nBGs samples after doping was done with scanning electron microscopy (SEM, Thermo Fisher Scientific, Apreo LoVac, USA), and global composition was determined using energy-dispersive X-ray spectroscopy (EDX). Further EDX (Thermo Fisher Scientific, Apreo LoVac, USA) measurements of the laser-doped nBGs composition on a single particle level were performed using Cs-corrected transmission electron microscope Jeol 2200FS (Japan) operating at 200 kV acceleration voltage. The samples were prepared by evaporation of a droplet of nBGs solution on a carbon film-supported gold grid.

In vitro cell culture

hMSCs (PromoCell, Germany) at passage 3 were expanded in αMEM supplemented with 10% FBS, 2 mM L-glutamine, 0.2 mM ascorbic acid, 100 U mL^{-1} penicillin and 100 mg mL^{-1} streptomycin, and the cultures kept in a humidified atmosphere with 5% CO_2 at 37 °C. 5000 cells per cm^2 density and 1 mL in volume of cells at passage 4 suspending in cell culture media, were seeded in each well of 12-well cell culture plates. For proper adhesion, cell culture media were exchange after 24 hours incubation time. Tube formation assay was performed using HUVEC pooled from different donors (Lonza, Germany). Prior to the experiment, the cells were cultured in endothelial growth medium (EGM, Lonza, Germany) without VEGF supplementation at 37 °C and 5% CO_2.

Cytotoxicity

The cytotoxicity of nBGs, iron and copper ion laser-doped nBGs with (FeCu) and iron, copper, and strontium ions laser-doped nBGs (FeCuSr) at concentrations ranging from 25 to 100 µg mL^{-1} was determined by the MTT assay according to kit's instructions. hMSCs were seeded at 5000 cells per cm^2 density in 96-well plates. As the confluence reached 80–90%, hMSCs were exposed to freshly prepared media with nBGs at different concentrations. Cytotoxicity was assessed 72 hours after exposure of the cells to nBGs. At each time point, 10 µL of MTT reagent was added to each well, followed by 4 hours of incubation at 37 °C, 5% CO_2. Crystalized formazan were dissolved in 150 µL of isopropanol with 10% by volume Triton-X 100. Amount of dissolved formazan was immediately determined by absorption at 570 nm using a microplate reader (BIO-RAD microplate reader-550, USA). Wells without cells but with complete medium, nBGs, and MTT reagent were used as blank baseline. The average formazan

concentration for each condition was used to calculate based on standard curve of known formazan concentration.

Live/Dead assay was performed using Calcein-AM and Ethidium bromide staining according to the manufacturers protocol (ThermoFisher; L3224). The staining solution was then removed, cells were washed with PBS and fresh media was added. Cells were imaged with a Nikon Eclipse Ti-E microscope (Nikon Instruments Europe BV, the Netherlands) at 10x objective.

Alkaline phosphatase assay

To evaluate the osteogenic capabilities in suspension, nanoparticles were suspended in basic media (no osteogenic stimulants) at a concentration of 100 μg mL^{-1}. Cell culture medium was refreshed every 3 days. After 7, 14, and 21 days of culturing, the ALP activity was measured for all conditions. 100 nM dexamethasone was added into basic media to make osteogenic media (OM). hMSCs cultured in osteogenic medium (OM; 100 nM dexamethasone) were included as a positive control for all samples. Alkaline phosphatase (ALP) production of hMSCs were used to evaluate their osteogenic differentiation at days 7, 14, and 21 of culture. ALP levels were normalized with DNA content measured by CyQuant Cell Proliferation assay kit (Thermo Fisher Scientific, Germany). Cell lysis buffer were made by diluted provided with the kit concentrated lyse buffer at ration of 1:20 in PBS and RNAse A (Thermo Fisher Scientific, Germany) were added to achieved 0.1% volume/volume. After discarding cell culture media, the cell layers were washed once with PBS. Samples in 100 μL of PBS were then undergo 6 times of 5 minutes each freezing–thawing cycle. 200 μL of cell lysis buffer was then introduced to each well and the samples undergo two more times of 30 minutes freeze-thawing cycles. After thawing, each sample were transferred into Eppendorf tube. All the samples' volume were then equalized by adding more cell lysis buffer. To ensure complete lysis of the cells, samples were sonicated for 5 minutes and incubated for 60 minutes at RT. DNA content were then quantified by mixing 100 μL of cell lysate with 100 μL CyQuant GR dye in 96 well plate. After 15 minutes incubation, fluorescence signals of samples and standard DNA concentrations were measured using microplate reader (BIO-RAD microplate reader-550, USA). CDP-star solution (ready-to-use, Sigma Aldrich, Germany) was used to quantify ALP activity. 40 μL of each sample cell lysate was incubated with 200 μL of CDP-star solution in a white-bottom 96-well plate at RT for 30 minutes in the dark. After incubation, chemical luminescence signal were measured at 466 nm using a microplate reader (BIO-RAD microplate reader-550, USA). The ALP values of each sample, normalized to their total DNA content, were expressed as an x-fold increase compared to hMSCs cultured with non-osteogenic medium.

Mineralization assay

Mineralization by hMSCs was measured *via* calcium deposition after 28 days of culturing using Alizarin Red S (sodium alizarin sulphonate) staining. After cell media were removed, 4% PFA was used to fixed cells to the cell culture plate. Alizarin Red S were then added to stained calcium present within each well. Red S solution was prepared by dissolving 2 g of solid dye powder in 100 mL of bi-distilled water. Once the solid was completely dissolved, pH of solution was then adjusted to 4.2 by 0.1 mM ammonium hydroxide in bi-distilled water. Prior to staining, cells were first washed once with PBS, then twice with bi-distilled water. 200 μL Alizarin Red solution was added to each well and incubated for 15 minutes at RT. Sample were then washed thrice with bi-distilled water to remove excess dye. Staining was visualized and image were recorded under a microscope (Nikon SMZ-25, Nikon, Japan) with 10X magnification.

A quantification method was carried out by performing extraction of the dye by 10% (w/v) cetylpyridinium chloride (CPC) (Sigma Aldrich, Germany) in 10 mM sodium phosphate (pH 7.0). Alizarin Red dye were dissolved from the samples by adding 1 mL of CPC solution per well and incubated for 15 minutes at RT under constant shaking. Exact dye solution were then removed from the cell culturing plate. To quantified amount of dye exacted, 10 μL of the extracted dye was further diluted 10 folds with CPC solution and transferred to a 96-well plate and. The absorbance at 555 nm of violet-coloured supernatant was analysed with a microplate reader (CLARIOstar Multimode Microplate Reader, BMG Labtech, Germany). Concentration were then calculated based on standard curve of known calcium concentration solution.

In vitro angiogenesis- tube formation assay

HUVECs pooled from different donors were cultured in endothelial growth medium (EGMTM, Lonza, Germany) without VEGF supplementation at 37 °C and 5% CO_2. An *in vitro* tube formation assay was performed in 48 well tissue culture plates (NUNC, Thermo Fisher Scientific, Germany). Wells were coated with 50 μL per well Geltrex™ (Thermo Fisher Scientific, Germany) according to the manufacturer's instructions. The laser-doped nBGs particles were suspended in Geltrex at 0.25 mg mL^{-1}. Pure Geltrex and Geltrex with the addition of 100 ng mL^{-1} of VEGF served as controls. HUVECs at passage 3 were seeded at a density of 40 000 cells per cm^2 in EGM. After 12 hours of incubation, cells were washed twice with PBS and fixed with 4% PFA for 20 minutes. Then, cells were washed twice and stored at 4 °C for subsequent analysis.

Fluorescent staining and microscopy

Fixed cells were permeabilized with 0.1% TritonX-100 in PBS (200 μL/well) for 10 minutes and washed twice with PBS. Then, F-actin staining was performed by incubation with 50 μL per well of 1:200 PBS-diluted Alexa Fluor™ 488 phalloidin (Thermo Fisher Scientific) for 20 minutes in the dark, followed by two washing steps in PBS. Cell nuclei were stained by immersion in 50 μL per well of DAPI (Thermo Fisher Scientific, Germany) at a concentration of 0.5 μg mL^{-1} in PBS for 5 minutes, followed by a last washing step. Imaging was performed using an inverted Nikon Ti-E microscope (Nikon Instruments Europe BV, the Netherlands). Images were processed and analyzed using Nikon NIS-Elements Viewer 4.50, and quantitative analysis of *in vitro* tubule formation was performed using the AngioTool software.[41]

Statistical analysis

Statistical analysis of ALP activity and mineralization experiments were performed using triplicates ($n = 3$), and data is presented as mean ± standard deviation. To analyze the data regarding the osteogenic differentiation, statistical evaluation was performed using GraphPad Prism 9.1 using one-way ANOVA followed by Turkey's multiple comparisons and mean differences were considered statistically significant when $p < 0.033$. Statistical analysis of the tube-formation assay was performed using ordinary one-way ANOVA followed by Tukey's multiple comparison test. The level of significance was set to $p < 0.05$.

Conclusions

In this work, we show that nBGs could be successfully doped with Fe, Sr, and/or Cu using nanosecond-pulsed laser excitation in liquids. Furthermore, laser ion doping did not alter the morphology or size of the nBGs. This is critical as a size reduction could also alter the cellular response due to changes in overall BG surface area and solubility. nBGs and laser-doped nBGs were biocompatible up to 100 μg mL^{-1} and could significantly increase ALP production in hMSC cells compared to non-exposed hMSC cells. Non-doped nBGs and nBGs laser-doped with Fe, Cu, and Sr were most effective in inducing ALP activity. However, a reduction in ALP induction and mineralization was observed in FeCu-doped nBGs, likely due to the presence of Fe. Differential activity was observed in the *in vitro* tubular experiments; nBGs doped with FeSr led to significantly increased vessel area and number of junctions. This data shows that pulsed laser doping is a promising technique to dope multiple ions in nBGs without negatively impacting their structure or size and that laser doping of FeSr into nBGs can improve the angiogenic properties of nBGs.

Author contributions

Matthias Schumacher, Christoph Rehbock, Stephan Barcikowski and Sabine van Rijt: conceptualization. Pichaporn Sutthavas, Matthias Schumacher, Martyna Nikody, Vaijayanthi Ramesh and Jurij Jakobi: data curation, formal analysis, investigation and methodology, validation and visualization. Pamela Habibovic, Christoph Rehbock, Stephan Barcikowski and Sabine van Rijt: funding acquisition. Sabine van Rijt: project administration. Elizabeth R. Balmayora, Pamela Habibovic, Christoph Rehbock, Stephan Barcikowski and Sabine van Rijt: supervision. Pichaporn Sutthavas, Martyna Nikody, and Sabine van Rijt: writing – original draft. Sabine van Rijt: writing – review & editing.

Conflicts of interest

There are no conflicts to declare.

Acknowledgements

References

1 K. Zheng and A. R. Boccaccini, *Adv. Colloid Interface Sci.*, 2017, **249**, 363–373.

2 A. Hoppe, N. S. Güldal and A. R. Boccaccini, *Biomaterials*, 2011, **32**, 2757–2774.

3 C. H. Kong, C. Steffi, Z. Shi and W. Wang, *J. Biomed. Mater. Res., Part B*, 2018, **106**, 2878–2887.

4 I. Cacciotti, *J. Mater. Sci.*, 2017, **52**, 8812–8831.

5 A. M. El-Kady, A. F. Ali, R. A. Rizk and M. M. Ahmed, *Ceram. Int.*, 2012, **38**, 177–188.

6 M. Catauro, F. Papale, P. Caputo and G. Donnarumma, *Int. J. Appl. Ceram. Technol.*, 2017, **14**, 108–116.

7 A. Bari, N. Bloise, S. Fiorilli, G. Novajra, M. Vallet-Regí, G. Bruni, A. Torres-Pardo, J. M. González-Calbet, L. Visai and C. Vitale-Brovarone, *Acta Biomater.*, 2017, **55**, 493–504.

8 P. Naruphontjirakul, A. E. Porter and J. R. Jones, *Acta Biomater.*, 2018, **66**, 67–80.

9 P. Sutthavas, M. Schumacher, K. Zheng, P. Habibović, A. R. Boccaccini and S. van Rijt, *Nanomaterials*, 2022, **12**, 2918.

10 S. van Rijt, K. de Groot and S. C. Leeuwenburgh, *Tissue Eng.*, 2022, **28**, 461–477.

11 N. Pajares-Chamorro and X. Chatzistavrou, *ACS Omega*, 2020, **5**, 12716–12726.

12 L. M. Frias Batista, A. Nag, V. K. Meader and K. M. Tibbetts, *Sci. China: Phys., Mech. Astron.*, 2022, **65**, 1–45.

13 A. Chemin, J. Lam, G. Laurens, F. Trichard, V. Motto-Ros, G. Ledoux, V. Jarý, V. Laguta, M. Nikl and C. Dujardin, *Nanoscale Adv.*, 2019, **1**, 3963–3972.

14 C. H. Chen, D. Wu, Z. Li, R. Zhang, C. G. Kuai, X. R. Zhao, C. K. Dong, S. Z. Qiao, H. Liu and X. W. Du, *Adv. Energy Mater.*, 2019, **9**, 1803913.

15 L. Shang, J. Q. Wang, C. Q. Cheng, Y. Zhang, F. F. Zhang, Y. M. Xie, J. D. Lu, J. Mao, Q. J. Guo and C. K. Dong, *J. Alloys Compd.*, 2021, **874**, 159909.

16 F. F. Zhang, C. Q. Cheng, J. Q. Wang, L. Shang, Y. Feng, Y. Zhang, J. Mao, Q. J. Guo, Y. M. Xie and C. K. Dong, *ACS Energy Lett.*, 2021, **6**, 1588–1595.

17 S. Zerebecki, K. Schott, S. Salamon, J. Landers, E. Budiyanto, H. Wende, H. Tüysüz, S. Barcikowski and S. Reichenberger, *J. Phys. Chem. C*, 2022, **126**(36), 15144–15155.

18 Y. Li, V. Ramesh, F. Bider, N. Bradshaw, C. Rehbock, A. R. Boccaccini and S. Barcikowski, *J. Biomed. Mater. Res., Part A*, 2022, **110**, 1537–1550.

19 B. Kołodziejska, N. Stępień and J. Kolmas, *Int. J. Mol. Sci.*, 2021, **22**, 6564.

20 M. Šalandová, I. A. van Hengel, I. Apachitei, A. A. Zadpoor, B. C. van der Eerden and L. E. Fratila-Apachitei, *Adv. Healthcare Mater.*, 2021, **10**, 2002254.

21 C. Giacomelli, M. L. Trincavelli, C. Satriano, Ö. Hansson, D. La Mendola, E. Rizzarelli and C. Martini, *Int. J. Biochem. Cell Biol.*, 2015, **60**, 185–196.

22 H. Shi, S. Yang, S. Zeng, X. Liu, J. Zhang, T. Wu, X. Ye, T. Yu, C. Zhou and J. Ye, *Appl. Mater. Today*, 2019, **15**, 100–114.

23 M. Schumacher, P. Habibović and S. van Rijt, *ACS Appl. Mater. Interfaces*, 2022, **14**, 4959–4968.

24 G. Nikiforuk and L. Sreebny, *J. Dent. Res.*, 1953, **32**, 859–867.

25 M. Spellauge, M. Tack, R. Streubel, M. Miertz, K. S. Exner, S. Reichenberger, S. Barcikowski, H. P. Huber and A. R. Ziefuss, *Small*, 2023, **19**, 2206485.

26 S. Siekierski, *Comments Inorg. Chem.*, 1997, **19**, 121–131.

27 D. W. Smith, *J. Chem. Educ.*, 1977, **54**, 540.

28 M. Vallet-Regí, M. Colilla, I. Izquierdo-Barba, C. Vitale-Brovarone and S. Fiorilli, *Pharmaceutics*, 2022, **14**, 2636.

29 H. Zhu, K. Zheng and A. R. Boccaccini, *Acta Biomater*, 2021, **129**, 1–17.

30 N. Gupta, D. Santhiya, S. Murugavel, A. Kumar, A. Aditya, M. Ganguli and S. Gupta, *Colloids Surf., A*, 2018, **538**, 393–403.

31 A. El-Fiqi and H.-W. Kim, *Mater. Lett.*, 2021, **294**, 129759.

32 Y. F. He, Y. Ma, C. Gao, G. Y. Zhao, L. L. Zhang, G. F. Li, Y. Z. Pan, K. Li and Y. J. Xu, *Biol. Trace Elem. Res.*, 2013, **152**, 292–296.

33 Q. Yang, J. Jian, S. B. Abramson and X. Huang, *J. Bone Miner. Res.*, 2011, **26**, 1188–1196.

34 E. Balogh, E. Tolnai, B. Nagy Jr, B. Nagy, G. Balla, J. Balla and V. Jeney, *Biochim. Biophys. Acta, Mol. Basis Dis.*, 2016, **1862**, 1640–1649.

35 A. A. Gorustovich, T. Steimetz, R. L. Cabrini and J. M. Porto López, *J. Biomed. Mater. Res., Part A*, 2010, **92**, 232–237.

36 E. Gentleman, Y. C. Fredholm, G. Jell, N. Lotfibakhshaiesh, M. D. O'Donnell, R. G. Hill and M. M. Stevens, *Biomaterials*, 2010, **31**, 3949–3956.

37 S. Li, M. Wang, X. Chen, S. Li, J. Li-Ling and H. Xie, *Cell Proliferation*, 2014, **47**, 81–90.

38 J. Zhang, H. Shi, J. Liu, T. Yu, Z. Shen and J. Ye, *J. Mater. Chem. B*, 2015, **3**, 8782–8795.

39 F. Zhao, B. Lei, X. Li, Y. Mo, R. Wang, D. Chen and X. Chen, *Biomaterials*, 2018, **178**, 36–47.

40 M. Lau and S. Barcikowski, *Appl. Surf. Sci.*, 2015, **348**, 22–29.

41 E. Zudaire, L. Gambardella, C. Kurcz and S. Vermeren, *PLoS One*, 2011, **6**, e27385.